Check for updates

ADVANCED MATERIALS INTERFACES
www.advmatinterfaces.de

Liquid-Metal-Enabled Flexible Metasurface with Self-Healing Characteristics

*Arkadeep Mitra, Kevin Xu, Sachin Babu, Jun H. Choi, and Jeong-Bong Lee**

A flexible self-healing metasurface using gallium-based liquid metal encapsulated in polydimethylsiloxane (PDMS) operating in the X-band (8–12 GHz) is reported. A band-stop metasurface with center frequency at 9.82 GHz is designed using floating patches surrounding the respective end cap of a Jerusalem cross. A large-scale (up to 10 × 10 array) metasurface is patterned in PDMS and a rapid manufacturing method of vacuum filling using ultra-low pressure is used to yield parallel encapsulation of liquid metal in PDMS. The fabricated metasurface is physically flexible and its flexibility is repeatedly tested for bendability, stretchability (up to ≈89.13%), twistability, and foldability. Transmission characteristics of the flexible metasurface are measured in waveguide and free-space environments and it is found that the band-stop center frequency agrees well with the design. The flexible metasurface also is tested for its repairability and self-healing characteristics. The metasurface is partially or fully cut at certain part and the partial/full cut part of the metasurface is repaired by applying external pressure or using Kapton tape/UV glue. Those repaired metasurfaces show restoration of original transmission characteristics with minimal shift in frequency and magnitude.

1. Introduction

Gallium-based liquid metals, including EGaIn (a binary alloy of gallium 85.8% and indium 14.2%)[1] and galinstan (a ternary alloy of gallium 68.5%, indium 21.5%, and tin 10%)[2] fall under the zinc group of metals besides the well-known mercury. Gallium-based liquid metals exhibit low melting points (EGaIn: 15.4 °C, galinstan: 13.2 °C),[2] limitless deformability,[3] extremely low vapor pressure,[4] elevated boiling point (1300 °C),[4] and high electrical (3.4×10^6 S m^{-1} at 20 °C)[4] and thermal conductivity (16.5 W m-K^{-1} at 20 °C).[5] Moreover, in comparison to mercury, gallium-based liquid metal is nontoxic and biocompatible, and thus the more favorable of the two.[6] As an emerging material, liquid metal when used in combination with polydimethylsiloxane (PDMS) finds applications in soft/flexible and wearable electronics.[2] Due to its flexibility and deformability, liquid metal encapsulated in PDMS has recently shown self-healing characteristics after damage on the device.[7–9] Gallium-based liquid metal has been explored in various applications ranging from electrocardiogram,[10] microcooling,[11] thermometers,[12] flexible electrodes,[13,14] flexible interconnection,[15] strain sensors,[16] pressure sensors,[17] inkjet printing,[18] energy harvesting,[19,20] and magneto-hydrodynamic pumps.[21]

Metasurface-based frequency selective surface (FSS) exists in 1D or 2D as periodic arrays of sub-wavelength metallic elements on dielectric surfaces.[22,23] Based on material, physical construction,[24] and geometry,[25] the FSSs are classified into high-pass, low-pass, band-pass, and band-stop filter.[25,26] The performance and behavior of the FSS is dependent on the geometry, periodicity, array size, and choice of materials (conductivity and permittivity).[24] The FSSs have been extensively studied[27] since 1960s, however its fundamental origin can go back to Marconi and Franklin's patent of reflectors in 1919.[28] The ability to tailor FSSs to curtail certain frequency band makes it a vital component in communication applications including radar,[23,29,30] microwave absorber,[29] satellite,[23,31] electromagnetic interference shielding,[32] dichroic sub reflectors,[33] reflect array lenses,[34] lens antenna,[35] polarizers,[36] stealth blankets,[37] and wireless networks.[23,38]

Traditional metasurfaces have been realized on rigid substrates using materials such as glass,[23] quartz,[39] polytetrafluoroethylene (PTFE) reinforced with glass,[40] commercially available FR-4-based printed circuit boards,[41–43] Rogers 5880 PTFE composites supported with glass microfibers.[44] The varactor diodes like BB 837 or BB 857-02 V,[41,45] liquid crystal,[40,46] and silver paint were either soldered,[41] filled/deposited,[40,46] or painted into these mechanically rigid substrates.[23,47] Recently, liquid metal injection in all connected microfluidic channels in PDMS has been used to realize physically flexible metasurfaces with or without incorporation of soldered chip resistors.[48,49] While the metasurface is flexible, serial injection/withdrawal of liquid metal in all connected microfluidic channels may limit its application (e.g., metasurface that needs unconnected patterns). Injection filling is also known for leaving airgaps and may cause device delamination.[50]

A. Mitra, S. Babu, J.-B. Lee
Department of Electrical and Computer Engineering
University of Texas at Dallas
Richardson, TX 75080, USA
E-mail: jblee@utdallas.edu
K. Xu, J. H. Choi
Department of Electrical Engineering
University at Buffalo
Buffalo, NY 14260, USA
The ORCID identification number(s) for the author(s) of this article can be found under https://doi.org/10.1002/admi.202102141.

DOI: 10.1002/admi.202102141

 © 2022 Wiley-VCH GmbH

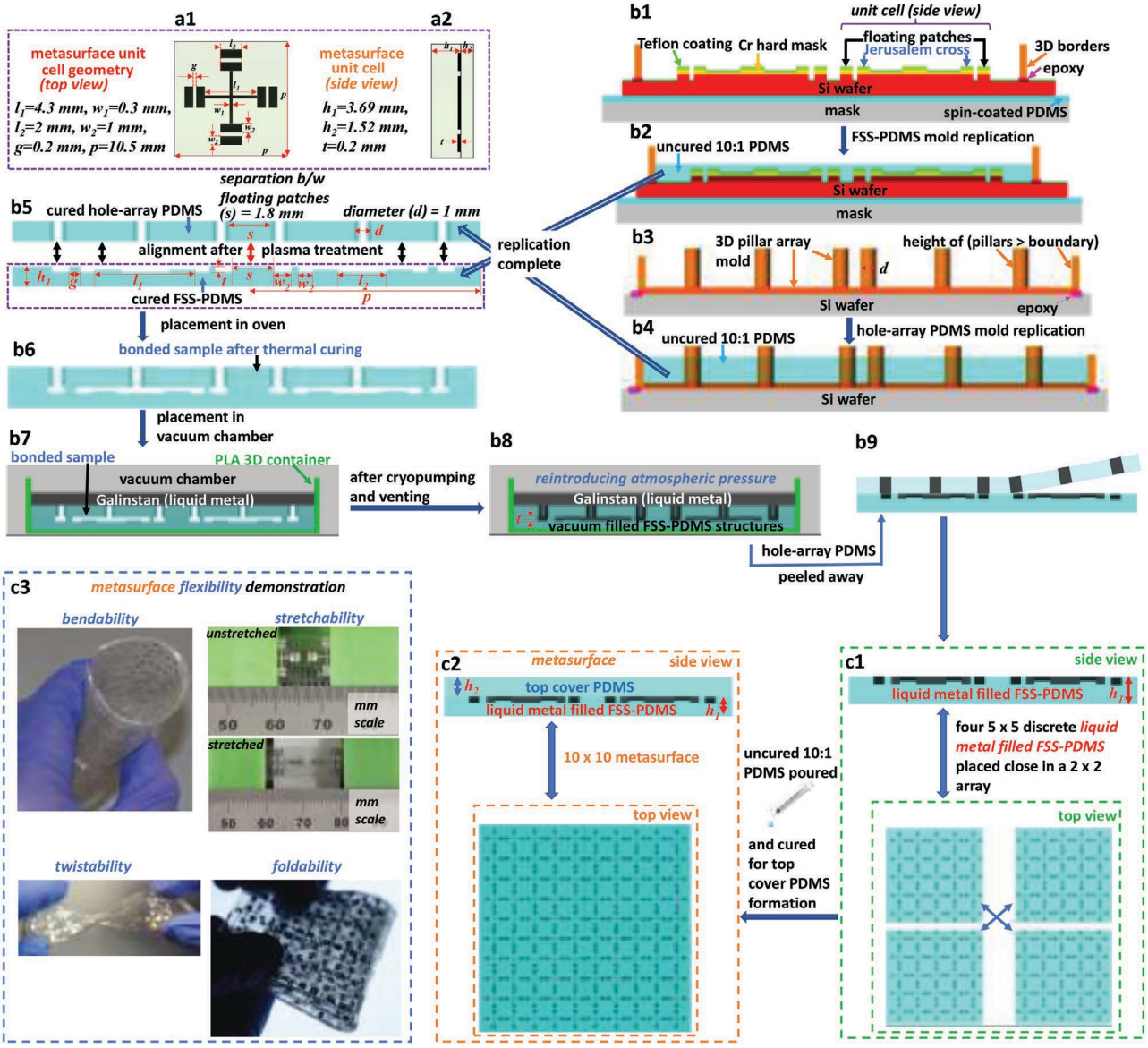

Figure 1. Liquid metal band-stop metasurface unit cell in PDMS. a1) Metasurface unit cell geometry involving modified Jerusalem cross layer (l_1 = 4.3 mm, w_1 = 0.3 mm, l_2 = 2 mm, w_2 = 1 mm, g = 0.2 mm, and p = 10.5 mm). a2) Side view of metasurface unit cell (h_1 = 3.69 mm, h_2 = 1.52 mm, t = 200 µm). b) Fabrication sequence of metasurface in ultra-low pressure. b1) 3D borders attached to the Teflon-coated plasma-etched Si wafer by using epoxy. b2) Uncured (10:1) PDMS poured on Si mold. b3) 3D pillar array mold (d = 1 mm) attached to the Si wafer by using epoxy. b4) PDMS poured on pillar array mold. b5) Alignment of the cured hole-array PDMS on cured FSS-PDMS after plasma treatment. b6) Bonded sample after thermal curing. b7) 3D container flooded with galinstan after placement of bonded structure in vacuum chamber. b8) Vacuum filling completion after cryopumping and reintroducing atmospheric pressure. b9) Hole-array PDMS peeled away from the liquid metal-filled metasurface samples. c) Characterization samples. c1) Side view of the liquid metal-filled FSS-PDMS and top view showing four 5 × 5 discrete liquid metal-filled FSS-PDMS placed close in a 2 × 2 array. c2) Side view and top view of the metasurface with cured top cover PDMS, formed by dispensing the uncured (10:1) PDMS from 1 mL syringe over the liquid metal-filled FSS-PDMS layer, followed by thermal and room temperature curing. c3) Flexibility demonstration of the metasurface in the form of bendability, stretchability, twistability, and foldability.

In this paper, we report high-throughput rapid manufacturing of a large (up to 10 × 10) array of physically flexible (bendable, stretchable, twistable, and foldable) self-healing metasurface designed to be operated in the X-band using galinstan liquid metal encapsulated in PDMS. Repairability and self-healing of the flexible metasurface have been tested and the repaired/self-healed flexible metasurface showed that its transmission characteristics have been completely restored.

2. Results and Discussions

The flexible metasurface in this work was based on Jerusalem cross resonator (**Figure 1**a), one of the common designs of FSSs. The metasurface pattern was designed to have 200 µm thickness (t) galinstan embedded in PDMS. At each of the four end caps (l_2 = 2 mm, w_2 = 1 mm, t = 0.2 mm) of the Jerusalem cross, liquid metal floating patches of the same size (l_2 = 2 mm,

© 2022 Wiley-VCH GmbH

w_2 = 1 mm, t = 0.2 mm) were placed with gap (g) of 200 µm. The crossed dipoles had identical length (l_1 = 4.3 mm) and width (w_1 = 0.3 mm). The size of the individual metasurface unit cell ($p \times p \times t$) encasing the Jerusalem cross and each of the four floating patches was 10.5 mm × 10.5 mm × 0.2 mm. The metasurface unit cell geometry (h_1 = 3.69 mm) with the additional top cover PDMS layer (h_2 = 1.52 mm) was modeled in ANSYS HFSS (high-frequency structure simulator) with galinstan (conductivity $\sigma = 3.46 \times 10^6$ S m^{-1}) encapsulated in PDMS (permittivity $\varepsilon_r = 2.3$ and loss tangent tan $\delta = 0.02$) (Figure 1a2). Periodic boundary conditions were applied to simulate the metasurface as an infinite 2D array.

Fabrication of the metasurface was started by patterning a Si wafer to create a mold for a 5 × 5 array of metasurface unit cell which consisted of inverse image of the Jerusalem cross resonator and four floating patches (Figure 1b1). The patterned Si mold was used to replicate PDMS for the 5 × 5 array metasurface (Figure 1b2). For an efficient injection of liquid metal into the discrete metasurface patterns, a 3D-printed pillar array mold (d = 1 mm) was fabricated for the replication of the hole-array PDMS (Figure 1b3,b4). The separation (s) between floating patches of neighboring unit cells was 1.8 mm (Figure 1b5). The hole-array PDMS was plasma bonded to the replicated PDMS of the 5 × 5 metasurface unit cell array (Figure 1b5,b6). Liquid metal filled the recessed PDMS patterns of the bonded metasurface by vacuum filling mechanism.[50] In this step, the bonded 5 × 5 metasurface unit cell array with liquid metal filling hole-array PDMS was placed in a 3D-printed polylactic acid (PLA) container and liquid metal was flooded in the container and it was placed in a vacuum chamber (Figure 1b7). The chamber was operated in ultra-low pressure (in the range of 10^{-6} Torr). Approximately 2 h of pumping allowed trapped air to fizz out from the metasurface PDMS patterns. The gas permeable PLA 3D container also aided in the air removal process.[51] Reintroducing atmospheric pressure caused the liquid metal to be filled into the massively parallel unconnected metasurface PDMS patterns via the hole-array PDMS (Figure 1b8) (see Experimental Section for details). Following vacuum filling, the bonded structure was cleaned and the hole-array PDMS was peeled off (Figure 1b9) to make multiple numbers of 5 × 5 metasurface array (Figure 1c1). A 10 × 10 array flexible metasurface was fabricated by assembling 2 × 2 set of the 5 × 5 array uncovered metasurface using PDMS top cover layer (h_2) (Figure 1c2). Since the fabricated metasurface only consists of liquid metal and PDMS, the metasurface is physically flexible. Repeated experiments of folding, bending, stretching (up to ≈89.13%), and twisting on the fabricated metasurface were carried out (Figure 1c3). Despite repeated bending, stretching, twisting, and folding, the metasurface sample remained intact.

Transmission and reflection characteristics of the fabricated flexible metasurface were measured using WR-90 waveguide (**Figure 2**a1). Due to the limited dimension of the WR-90 waveguide, Arconic MIC 6 cast aluminum sheet was milled to have an opening window (10.16 mm × 22.86 mm) and a 1 × 2 metasurface array was placed in the window of the sample holder. Two ports of a Keysight N542A PNA-X network analyzer were connected through waveguide to coax adapters to measure S-parameters calibrated up to the sample (Figure 2a1). Figure 2a2 shows measured and simulated band-stop characteristics of the flexible metasurface. The measured band-stop resonance frequency was turned out to be 9.5 GHz, slightly deviated from that of the simulation (9.82 GHz).

To test repairability and self-healing characteristics of the fabricated flexible metasurface, multiple numbers of 1 × 2 array flexible metasurface were subjected to various intentional physical damages. Figure 2b1 shows a sample 1 with cutting along the center of the 300 µm wide horizontal dipole (w_1, Figure 1a1) of one unit cell in the 1 × 2 array. In the sample 1, the cut caused the leakage of the liquid metal and thereby discontinuity between the top and bottom severed halves of the Jerusalem cross dipoles (Figure 2b2), thus creating an open circuit (Figure 2b3). As a result, the transmission and reflection characteristics were substantially altered (Figure 2b4). The damaged metasurface was self-healed by applying external pressure on the top cover PDMS (h_2, Figure 1c2) covering the region of the damage. The external pressure causes the viscoelastic oxide skin to rupture allowing the liquid metal to flow into the broken void spaces and reconnect (Figure 2b6,b7) (see a video S1 in the Supporting Information). The repaired sample showed nearly identical transmission/refection characteristics before damage with its resonant frequency shifted only 0.84% (9.42 GHz) (Figure 2b8). Another set of samples was cut along the vertical dipole of 1 × 2 unit cells (Figure 2c1) and repaired with Kapton tape (sample 2) (Figure 2c2) or an UV curing glue (sample 3) (Figure 2c3). The UV curing glue or Kapton tape was applied at the top and bottom side of the damaged region. These simple repairs restored flexible metasurface characteristics yielded a resonant frequency of 9.72 GHz (2.32% shifted) for the sample 2 (Kapton tape repaired sample) and 9.81 GHz (3.26% shifted) for the sample 3 (UV curing glue repaired sample) (Figure 2c4). Another set of samples were cut in the middle of the 1.8 mm separation (s) between the neighboring liquid metal floating patches of the 1 × 2 array (Figure 2d1) and repaired with Kapton tape (sample 4) (Figure 2d2) or an UV curing glue (sample 5) (Figure 2d3). The UV curing glue or Kapton tape was again applied at the top and bottom side of the damaged region. The repaired flexible metasurface samples yielded a resonant frequency of 9.57 GHz (0.74% shifted) for the sample 4 (Kapton tape repaired sample) and 9.58 GHz (0.84% shifted) for the sample 5 (UV curing glue repaired sample) (Figure 2d4).

The 10 × 10 fabricated metasurface sample (Figure 1c2) was mounted onto a sample holder and inserted into a window in the center of the metal foil backed PolyPro foam board (**Figure 3**a,b). A couple of Pasternack PE9887-11 horn antennas were placed on either side of the board for free-space characteristics measurement (Figure 3a). To prevent undesired reflection back toward the transmitting antenna, absorber panels (Eccosorb AN-75) were added to the PolyPro foam board (Figure 3c). The 3D-printed sample holder was designed to have a rotatable inner frame and an outer frame (Figure 3d). Measurements were repeated by rotating the sample mounted frame (Figure 3e), at different angles of oblique incidence ($0° \leq \theta_{inc} \leq 45°$) for both transverse electric (TE) polarization and transverse magnetic (TM) polarization. Copper tape was added around the edges of the 3D-printed sample holder to prevent leakage during the transmission coefficient measurement at oblique angles of incidence (Figure 3e). Resonant frequency

© 2022 Wiley-VCH GmbH

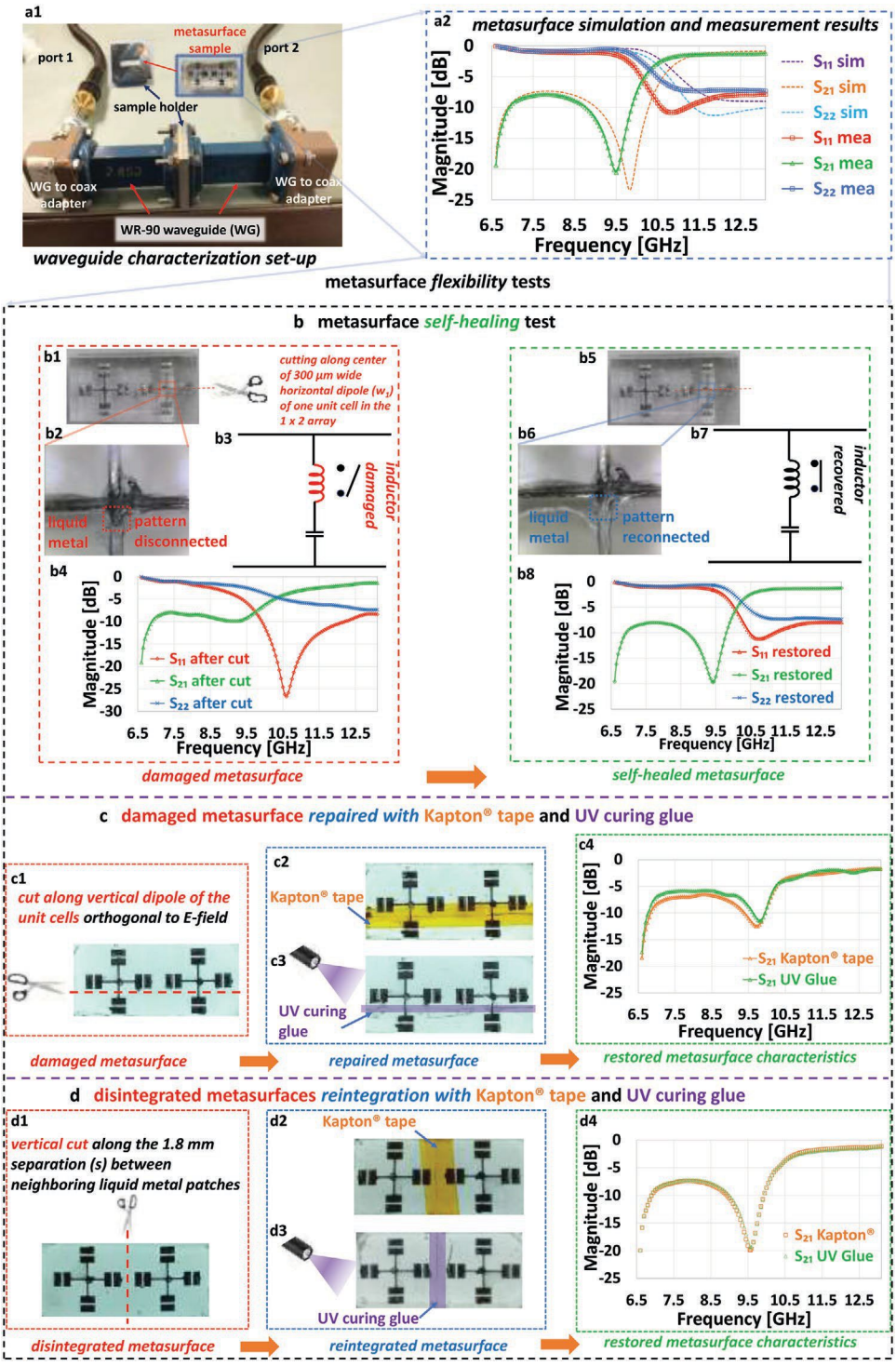

Figure 2. Waveguide-based metasurface flexibility tests. a1) Waveguide characterization set-up for the 1 × 2 metasurface sample using WR-90 waveguide. a2) Metasurface simulation (sim) and measurement (mea) results. b) Illustrates the metasurface self-healing test on sample one. b1) Cutting along the center of the 300 µm wide horizontal dipole (w_1) of one unit cell in the 1 × 2 array. b2) Zoomed-in view of the crossed dipoles showing loss of liquid metal due to cutting. b3) Series LC circuit disruption due to liquid metal loss from dipoles. b4) Loss of metasurface characteristics due to cutting. b5) Applying external pressure on the top cover PDMS of the half cut 1 × 2 sample. b6) Zoomed-in view showing liquid metal pattern reconnection in vacant spots due to the external pressure applied. b7) Recovered LC circuit. b8) Restored metasurface characteristics for sample 1. c) Shows the damaged metasurfaces repair test with Kapton tape and UV curing glue. c1) Cut along vertical dipole of the unit cells orthogonal to the E-field. c2) Kapton tape repairing for sample 2. c3) UV glue repairing for sample 3. c4) Restored metasurface characteristics of samples 2 and 3. d) Demonstrates the disintegrated metasurfaces reintegration with Kapton tape and UV curing glue. d1) Vertical cut along the 1.8 mm separation (s) between neighboring liquid metal patches. d2) Kapton tape repairing for sample 4. d3) UV glue repairing for sample 5. d4) Restored metasurface characteristics of samples 4 and 5.

© 2022 Wiley-VCH GmbH

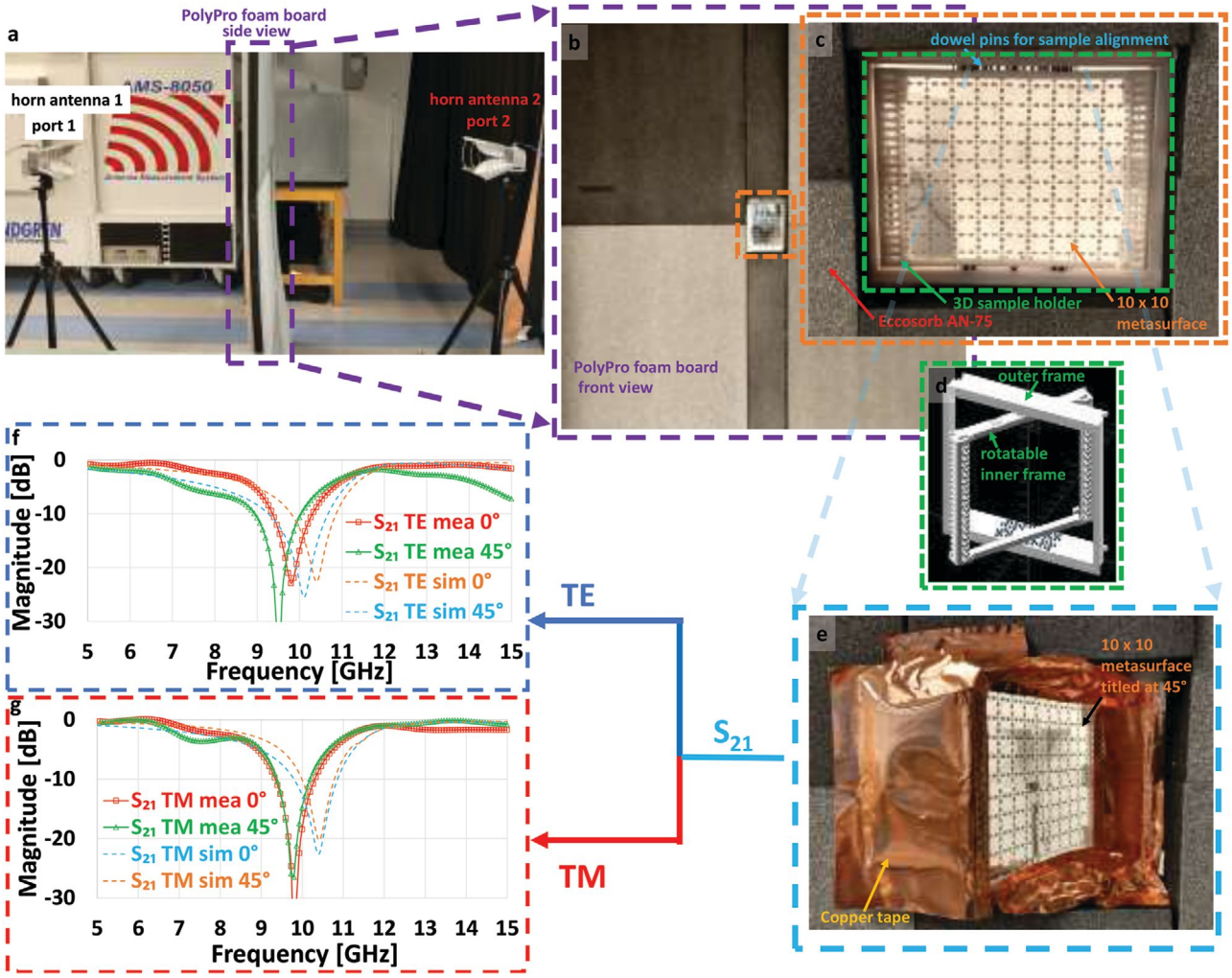

Figure 3. Free-Space setup and measurements. a) Side view of the PolyPro foam board holding the 10 × 10 metasurface sample in-between two horn antennas with respect to the board. b) Front view of the PolyPro foam board holding the 10 × 10 metasurface sample. c) 3D-printed sample holder for holding the 10 × 10 metasurface sample with dowel pins for sample alignment surrounded by absorber panels: Eccosorb AN-75 on the metallic foil side of the PolyPro foam board to prevent undesired reflection. d) 3D-printed sample holder showing the rotatable inner frame with respect to the outer frame. e) 10 × 10 metasurface sample rotated at 45° angle of incidence with copper tape wrapped around edges to avoid leakage during transmission measurements at oblique angles of incidence. f) S_{21} TE measurement (mea) and simulation (sim) results at 0° and 45°. g) S_{21} TM measurement (mea) and simulation (sim) results at 0° and 45°.

for the measured TE polarization varied between 9.53 GHz (at 45°) and 9.8 GHz (at 0°) (Figure 3f). Measurements were repeated for TM polarization by rotating the horn antennas by 90°. Resonant frequency for the measured TM polarization was measured to be 9.8 GHz (at 0° and 45°) (Figure 3g).

3. Conclusion

In conclusion, the highly repeatable vacuum filling process was demonstrated for complete filling in complex geometry of the 5 × 5 FSS unconnected patterns with gallium-based liquid metal. During waveguide measurements by inflicting intentional damages, the transmission response of metasurface was lost. Invoking the self-healing via external pressure on top cover PDMS (by causing rupture of viscoelastic gallium oxide membrane) recovered liquid metal pattern continuity in damaged spaces and thereby restored metasurface transmission responses. Additional metasurface was subjected to damages in vertical dipole and band-stop center frequency was obtained after repairing the damaged metasurface with Kapton tape and UV glue. Discrete metasurface joining was also carried out by cutting the 1 × 2 metasurface array along the 1.8 mm gap between neighboring floating patches. The measurement results from the free-space characterization agreed well with the simulation results. The ability of making highly resilient large array (10 × 10), physically flexible and repairable metasurface may enable unique field-deployable metasurface in communication and military applications. Although, the floating patches are fixed in our design, we envision to make these patches dynamically tunable in an extended work.

© 2022 Wiley-VCH GmbH

4. Experimental Section

Fabrication and Bonding of 5 × 5 FSS-PDMS and Hole-Array PDMS: ME03 Temescal E-gun Evaporator (Ferrotech Temescal Systems, Livermore, CA, USA) was used for the deposition of 1200 Å thick chromium (Cr) on top of the MicroChem S1813 (Kayaku Advanced Materials, Inc., Westborough, MA, USA) patterned 4" Si wafer (University Wafer Inc., Boston, MA, USA). S1813 liftoff yielded Cr hard mask over Si. Deep Si etching was done using PE04 PlasmaTherm ICP Fluorine Etcher (Plasma-Therm, LLC, St. Petersburg, FL, USA) for a total etch depth of 200 µm. Teflon (C_4F_8) was coated on the etched Si wafer to complete the etching process. Sylgard 184 (Dow Chemical, Midland, MI, USA) uncured 10:1 PDMS was spin coated on the glass side of a mask and Teflon-coated Si wafer was placed over it. Complete thermal curing was done in an oven at 95 °C for 15–20 min. A square-shaped border with height of 2 mm was glued on the borders of the Si wafer using Devcon 5 Minute Epoxy (ITW Performance Polymers, Danvers, MA, USA). The border was printed using a Photon S (Hongkong Anycubic Technology Co., Ltd., Tsim Sha Tsui, Kowloon, China) 3D printer consisting of Anycubic's stereolithography (SLA)-based EC UV Resin (UV wavelength: 355–410 nm) materials. Sylgard 184 uncured 10:1 PDMS was poured on the FSS-Si mold and complete curing was done in a hotplate at 96 °C for 20 min. The cured FSS-PDMS (h_1 = 3.69 mm) was peeled from the FSS-Si mold. Pillar array with pillar diameter (d) of 1 mm was bonded to the Si wafer by using Devcon 5 Minute Epoxy. The pillar array was 3D printed with SLA-based resin materials. Sylgard 184 uncured 10:1 PDMS was poured on the SLA 3D-printed pillar array by using a 1 mL syringe (Brandzig, Monsey, NY, USA). The hole-array PDMS in the pillar array mold was cured in an oven at 95 °C for 8.5–9.5 min. Once removed from the oven, cooling time of 1–2 min was allowed following which the hole-array PDMS was peeled off. The FSS-PDMS and the hole-array PDMS were aligned, and plasma was bonded after being exposed to oxygen plasma in Trion Sirius-T2 RIE Etcher (Trion Technology, Tempe, AZ). Following bonding, thermal curing was done in an oven at 115 °C for 2–2.5 h. After curing, cooling at room temperature was allowed for 2–3 min.

Vacuum Filling: The bonded 5 × 5 metasurface unit cell array was placed in an open top container printed with a fused deposition modeling (FDM) Qidi Tech (Zhejiang Qidi Technology Co., Ltd., Ruian, Zhejiang Province, China) 3D printer comprising of PLA filament materials (IPSG, Hilliard, OH, USA). In the 3D-printed PLA container, the hole-array PDMS was facing upward. Galinstan (Ga 68.5%, In 21.5%, Sn 10%, Changsha Rich Nonferrous Metals Co., Ltd., Hunan, China) was flooded into the 3D-printed container. To avoid contamination in the vacuum chamber, the 3D container was placed inside a glass container (Killdee Scientific Glass Company Inc., Santa Fe Springs, CA, USA). This glass container was loaded into ME03 Temescal E-gun evaporator at atmospheric pressure. Pressure in the evaporator dropped to 5.75×10^{-6} Torr after 45 min. After a vacuum period of 2 h, the high vacuum valve was closed, and venting was allowed to let vacuum filling take place for the metasurface sample. Following vacuum filling and cleaning, the hole-array PDMS was removed from the 5 × 5 metasurface sample. In the final fabrication step, Sylgard 184 uncured 10:1 PDMS was poured over the FSS-PDMS liquid metal filled structures to cover the metasurface with the top cover PDMS (h_2 = 1.52 mm). Thermal curing was done on a hotplate at 75 °C for 45 min followed by completed curing for ≈48 h at room temperature.

Waveguide Characterization and Repair: For the waveguide measurement, the 1 × 2 metasurface array was cut from the 5 × 5 metasurface sample and placed inside a window which was milled out of 6.35 mm thick Arconic MIC 6 cast aluminum sheet. The ports of the Keysight N542A PNA-X network analyzer (Keysight Technologies, Santa Rosa, CA, USA) were connected through the WR-90 waveguide (Pasternack, Irvine, CA, USA) to the coax adapters. Repairing of the cut samples was done by applying Kapton tape (DuPont, Wilmington, DE, USA) and UV glue (Visbella, City of Industry, CA, USA). The UV glue was cured inside an LPKF 200–247 UV Lamp Table (LPKF Laser & Electronics, Tualatin, OR, USA) for ≈2 min.

Free-Space Sample Fabrication and Characterization: A 2 × 2 set of 5 × 5 metasurface samples was assembled by placing them over a hotplate at 75 °C. 1 mL syringe was used for dispensing Sylgard 184 uncured 10:1 PDMS over the assembled samples. Thermal curing was done in a hotplate at 75 °C for 45 min followed by completed curing for ≈48 h at room temperature. The 10 × 10 array was placed in the 3D-printed rotatable inner frame with the fixed outer frame. The mounted sample was placed in a PolyPro metallic foil-backed expanded polystyrene (EPS) insulation foam board. Copper tape was added around the edges of the 10 × 10 sample to prevent leakage. To ensure that the PolyPro foam board was not tilted, a Fluke 424D laser distance meter was used for leveling. Pasternack PE9887-11 (Pasternack, Irvine, CA, USA) horn antennas were placed on either side of the sample. The positioning of the Pasternack PE9887-11 horn antennas with respect to the PolyPro foam board was determined by Fluke 424D laser distance meter, whereby the initial antenna position was determined and then viewing the time domain response to see the distance to the target from each antenna. The reflection coefficients were measured by placing the two Pasternack PE9887-11 horn antennas in Naval Research Laboratory (NRL) Arch style. The Pasternack PE9887-11 horn antennas were rotated symmetrically in arc around the 10 × 10 FSS sample at 15°, 30°, 45° to do the reflection coefficients (S_{11}, S_{22}) measurements.

Supporting Information

Supporting Information is available from the Wiley Online Library or from the author.

Acknowledgements

This work was supported in part by the United States National Science Foundation grant NSF ECCS—1908779. The authors acknowledge Dr. Ye Il Choi, Mohammad Salman Parvez, Jinwon Jeong, and UT Dallas Clean Room staff for their support on this work.

Conflict of Interest

The authors declare no conflict of interest.

Data Availability Statement

The data that support the findings of this study are available from the corresponding author upon reasonable request.

Keywords

flexible metasurface, liquid metal, PDMS, repairable metasurface, self-healing metasurface

Received: November 3, 2021
Revised: January 30, 2022
Published online: March 8, 2022

[1] M. D. Dickey, R. C. Chiechi, R. J. Larsen, E. A. Weiss, D. A. Weitz, G. M. Whitesides, *Adv. Funct. Mater.* **2008**, *18*, 1097.
[2] T. Daeneke, K. Khoshmanesh, N. Mahmood, I. A. de Castro, D. Esrafilzadeh, S. J. Barrow, M. D. Dickey, K. Kalantar-zadeh, *Chem. Soc. Rev.* **2018**, *47*, 4073.

© 2022 Wiley-VCH GmbH

[3] D. Kim, P. Thissen, G. Viner, D. W. Lee, W. Choi, Y. J. Chabal, J.-B. Lee, *ACS Appl. Mater. Interfaces* **2013**, *5*, 179.
[4] G. Li, M. Parmar, D. Kim, J.-B. Lee, D. W. Lee, *Lab Chip* **2014**, *14*, 200.
[5] C. Cao, X. Ma, X. He, J. Xu, J. Xie, G. Liu, *Int. Commun. Heat Mass Transfer* **2021**, *120*, 105019.
[6] M. Knoblauch, J. M. Hibberd, J. C. Gray, A. J. E. van Bel, *Nat. Biotechnol.* **1999**, *17*, 906.
[7] F. Krisnadi, L. L. Nguyen, Ankit, J. Ma, M. R. Kulkarni, N. Mathews, M. D. Dickey, *Adv. Mater.* **2020**, *32*, 2001642.
[8] G. Li, X. Wu, D.-W. Lee, *Sens. Actuators, B* **2015**, *221*, 1114.
[9] G. Li, X. Wu, D.-W. Lee, *Lab Chip* **2016**, *16*, 1366.
[10] R. Guo, X. L. Wang, W. Z. Yu, J. B. Tang, J. Liu, *Sci. China: Technol. Sci.* **2018**, *61*, 1031.
[11] K. Q. Ma, J. Liu, *J. Phys. D: Appl. Phys.* **2007**, *40*, 4722.
[12] L. S. Smith, *BMC Nurs.* **2003**, *2*, 1.
[13] N. Hallfors, A. Khan, M. D. Dickey, A. M. Taylor, *Lab Chip* **2013**, *13*, 522.
[14] J. H. So, M. D. Dickey, *Lab Chip* **2011**, *11*, 905.
[15] H. J. Kim, C. Son, B. Ziaie, *Appl. Phys. Lett.* **2008**, *92*, 011904.
[16] S. Yao, Y. Zhu, *Nanoscale* **2014**, *6*, 2345.
[17] Y. Gao, H. Ota, E. W. Schaler, K. Chen, A. Zhao, W. Gao, H. M. Fahad, Y. Leng, A. Zheng, F. Xiong, C. Zhang, L. C. Tai, P. Zhao, R. S. Fearing, A. Javey, *Adv. Mater.* **2017**, *29*, 1701985.
[18] D. Kim, J. H. Yoo, Y. Lee, W. Choi, K. Yoo, J.-B. Lee, in Proc. 2014 IEEE 27th Int. Conf. Micro Electro Mechanical Systems (MEMS), San Francisco, CA, USA **2014**, p. 967.
[19] W. Tang, T. Jiang, F. R. Fan, A. F. Yu, C. Zhang, X. Cao, Z. L. Wang, *Adv. Funct. Mater.* **2015**, *25*, 3718.
[20] J. Jeon, S. K. Chung, J.-B. Lee, S. J. Doo, D. Kim, *Eur. Phys. J.: Appl. Phys.* **2018**, *81*, 20902.
[21] M. Hodes, R. Zhang, L. S. Lam, R. Wilcoxon, N. Lower, *IEEE Trans. Compon., Packag., Manuf. Technol.* **2013**, *4*, 46.
[22] K. Payne, K. Xu, J. H. Choi, *IEEE Trans. Microwave Theory Tech.* **2018**, *66*, 4783.
[23] F. Bayatpur, *Ph.D. Thesis*, The University of Michigan, **2009**.
[24] R. S. Anwar, L. Mao, H. Ning, *Appl. Sci.* **2018**, *8*, 1689.
[25] R. Panwar, J.-R. Lee, *Aerosp. Sci. Technol.* **2017**, *66*, 216.
[26] A. Kapoor, R. Mishra, P. Kumar, *Alexandria Eng. J.* **2021**, *61*, 4263.
[27] S. B. Glybovski, S. A. Tretyakov, P. A. Belov, Y. S. Kivshar, C. R. Simovski, *Phys. Rep.* **2016**, *634*, 1.
[28] G. Marconi, C. S. Franklin, U.S. 1,301,473, **1919**.
[29] C. Davenport, J. Rigelsford, *Electron. Lett.* **2013**, *49*, 1478.
[30] C. Davenport, J. Rigelsford, *IEEE Trans. Antennas Propag.* **2014**, *62*, 4518.
[31] M. R. Chaharmir, J. Shaker, *IEEE Trans. Antennas Propag.* **2015**, *63*, 1255.
[32] M. Koohestani, R. Perdriau, M. Ramdani, J. Carlsson, *IEEE Trans. Electromagn. Compat.* **2020**, *62*, 2785.
[33] V. Agrawal, W. Imbriale, *IEEE Trans. Antennas Propag.* **1979**, *27*, 466.
[34] S. V. Hum, J. Perruisseau-Carrier, *IEEE Trans. Antennas Propag.* **2013**, *62*, 183.
[35] J. Thornton, P. Haines, *Electron. Lett.* **2007**, *43*, 5.
[36] J. Y. Yin, X. Wan, J. Ren, T. J. Cui, *Sci. Rep.* **2017**, *7*, 41505.
[37] C. Zhang, J. Yang, W. Yuan, J. Zhao, J. Y. Dai, T. C. Guo, J. Liang, G. Y. Xu, Q. Cheng, T. J. Cui, *J. Phys. D: Appl. Phys.* **2017**, *50*, 444002.
[38] M. Raspopoulos, S. Stavrou, *IEEE Trans. Antennas Propag.* **2011**, *59*, 2998.
[39] M. Safari, C. Shafai, L. Shafai, *IEEE Trans. Antennas Propag.* **2015**, *63*, 1014.
[40] V. Fusco, R. Cahill, W. Hu, S. Simms, *Electron. Lett.* **2008**, *44*, 37.
[41] S. Ghosh, K. V. Srivastava, *IEEE Trans. Antennas Propag.* **2017**, *65*, 4903.
[42] Y. Youn, S. Cho, H. J. Song, W. Hong, *IEEE Trans. Veh. Technol.* **2020**, *69*, 1719.
[43] J. Zhao, Q. Cheng, J. Chen, M. Q. Qi, W. X. Jiang, T. J. Cui, *New J. Phys.* **2013**, *15*, 043049.
[44] A. Hoque, M. T. Islam, A. F. Almutairi, M. E. H. Chowdhury, M. Samsuzzaman, *Sci. Rep.* **2020**, *10*, 13086.
[45] C. Jin, Q. Lv, B. Zhang, J. Liu, Z. S. He, Z. Shen, *IEEE Trans. Antennas Propag.* **2021**, *69*, 5673.
[46] D. Shrekenhamer, W. C. Chen, W. J. Padilla, *Phys. Rev. Lett.* **2013**, *110*, 177403.
[47] Q. Chen, F. Mesa, P. Padilla, X. Yin, O. Quevedo-Teruel, *IEEE Trans. Antennas Propag.* **2020**, *68*, 7777.
[48] S. Ghosh, S. Lim, *IEEE Trans. Microwave Theory Tech.* **2018**, *66*, 3857.
[49] H. K. Kim, D. Lee, S. Lim, *Sci. Rep.* **2016**, *6*, 31823.
[50] Y. Lin, O. Gordon, M. R. Khan, N. Vasquez, J. Genzer, M. D. Dickey, *Lab Chip* **2017**, *17*, 3043.
[51] H. J. Lehermeier, J. R. Dorgan, J. D. Way, *J. Membr. Sci.* **2001**, *190*, 243.

© 2022 Wiley-VCH GmbH